Prepared for submission to JINST

Development of a time correction algorithm for a precise synchronization of a free-running Rubidium atomic clock with the GPS Time

Claire Dalmazzone,[a,1] **Mathieu Guigue,**[a] **Lucile Mellet,**[a,2] **Boris Popov,**[a] **Stefano Russo,**[a] **Vincent Voisin,**[a]
Michel Abgrall,[b] **Baptiste Chupin,**[b] **Caroline Lim,**[b] **Paul Éric Pottie,**[b] **Pierre Ulrich**[b]

[a]*Laboratoire de Physique Nucléaire et de Hautes Energies (LPNHE), Sorbonne Université, CNRS/IN2P3, 4 place Jussieu, 75005 Paris, France*
[b]*LNE-SYRTE, Observatoire de Paris, Université PSL, CNRS, Sorbonne Université, 61 avenue de l'Observatoire, 75014 Paris, France*

E-mail: claire.dalmazzone@lpnhe.in2p3.fr

Abstract: We present results of our study devoted to the development of a time correction algorithm needed to precisely synchronize a free-running Rubidium atomic clock with the Coordinated Universal Time (UTC). This R&D is performed in view of the Hyper-Kamiokande (HK) experiment currently under construction in Japan, which requires a synchronization with UTC and between its different experimental sites with a precision better than 100 ns. We use a Global Navigation Satellite System (GNSS) receiver to compare a PPS and a 10 MHz signal, generated by a free-running Rubidium clock, to the Global Positioning System (GPS) Time signal. We use these comparisons to correct the time series (time stamps) provided by the Rubidium clock signal. We fit the difference between Rubidium and GPS Time with polynomial functions of time over a certain integration time window to extract a correction of the Rubidium time stamps in offline or online mode. In online mode, the latest fit results are used for the correction until a new comparison to the GPS Time becomes available. We show that with an integration time window of around 10^4 seconds, we can correct the time stamps drift caused by the frequency random walk noise of the free running Rubidium clock so that the time difference with respect to the GPS Time stay within a ± 5 ns range in both offline or online correction mode.

Keywords: timing detectors; precise timing; atomic clock; Rb; PHM; GPS; GNSS; UTC

[1]Corresponding author.
[2]Now at Michigan State University, Department of Physics and Astronomy, East Lansing, Michigan, USA

Contents

1 Introduction

A precise synchronization with the Coordinated Universal Time (UTC) or with another signal is a necessity in many applications, particularly in long-baseline physics experiments including several experimental sites. A good example is long-baseline neutrino oscillation experiments, like OPERA [1] (2006-2012), T2K [2] (from 2010) and NOvA [3] (from 2014), where a beam of neutrinos is produced and characterized in a first experimental site and detected, after several hundreds of kilometers of propagation, at another site to measure a change of the beam properties. Two next generation long-baseline neutrino experiments are being built at the moment: Hyper-Kamiokande (HK) [4] that plans to start taking data in 2027 and DUNE [5][6] that should begin sometime after 2029. These experiments require a synchronization of 100 ns or better between the different experimental sites. Moreover, multi-messenger programs that plan to compare different components of astrophysical events [7] (e.g.: gamma-ray bursts, gravitational waves, neutrino emissions of supernovae, etc.) require a synchronization with UTC of different experiments located all over the world. For instance, to enter the SuperNova Early Warning System (SNEWS) network [8], a synchronization to UTC better than 100 ns is required.

Many long-baseline physics experiments use atomic oscillators as frequency references because of their good short term stability. Among the reference oscillators available on the market, Rubidium atomic clocks are generally chosen for their affordability as it was the case for the T2K [9] and Super-Kamiokande [10] timing systems. However, Rubidium clocks usually drift away from a stable reference because of frequency drift and random walk. For synchronization to UTC, this drift usually needs to be prevented or corrected. A common solution is to discipline the average frequency of the clock to the signals of an external Global Navigation Satellite System (GNSS) receiver, with an integration time window chosen so that it does not deteriorate the short term stability of the clock. However, it presents some drawbacks like the fact that the user has little control on the setup. In case of problems (like jumps in the time comparison), it is difficult to understand where they come from (GPS Time, receiver, the master clock, etc.) and to assess the uncertainty on the synchronization to UTC. The R&D work presented in this paper and introduced in [11] is focused on designing and characterizing an alternative method that allows more freedom to the user and a better understanding of the process. It is based on known metrology techniques [12, 13]. The proposed method uses a free-running atomic clock to derive a time signal and provide time stamps. In a physics experiment these would be the time stamps of detected events. The time stamps are corrected in post-processing using comparisons of the Rubidium clock signal to GNSS Time. In that way, we can store all the information (the raw signal, the comparisons to GPS Time, the derived correction etc.) and apply the correction in either online (during the data-acquisition) or offline modes. Let us note that the GNSS time is a good approximation of the UTC, within a few nanoseconds, and it allows synchronization to UTC via a common-view technique [14]. The common-view would be performed with a national laboratory providing a local realization of UTC(k), like e.g. the NICT laboratory in Japan [15], then the conversion to UTC can be performed with the help of the Circular T of the BIPM (Bureau International des Poids et Mesures) [16] at the end of each month.

2 Materials and Methods

2.1 Experimental setup

The experimental setup that we used is schematized in Figure 1. It is located at the Pierre and Marie Curie (Jussieu) campus of the Sorbonne University in Paris. The setup consists of two main parts: one represents the timing generation and correction setup, that could be reproduced in the HK experiment, and the second part is related to testing the efficiency of the correction method. In the first part a Rubidium clock (Rb) in free-running mode, at the ground floor of the laboratory, generates a Pulse Per Second (PPS) signal and a 10 MHz signal that are transported to the fifth floor with the White Rabbit (WR) protocol. The timing signals of the slave WR switch are used by a GNSS receiver as a reference for its internal clock. The receiver connected to its antenna on the roof, above the fifth floor, is used to measure time comparisons between the GPS Time and the Rubidium clock. This physical distance between the time generation part and the receiver was done on purpose to mimic what would happen in many long-baseline physics experiments. Indeed, in Hyper-Kamiokande, the Rubidium clock would be placed inside a mountain where a cavern has been dug to host the detector whereas the receiver would have to be placed outside in a valley. The second part of our experimental setup is contained in the experimental room at the ground floor and its purpose is to validate the performance of the method, it would not be reproduced in the final

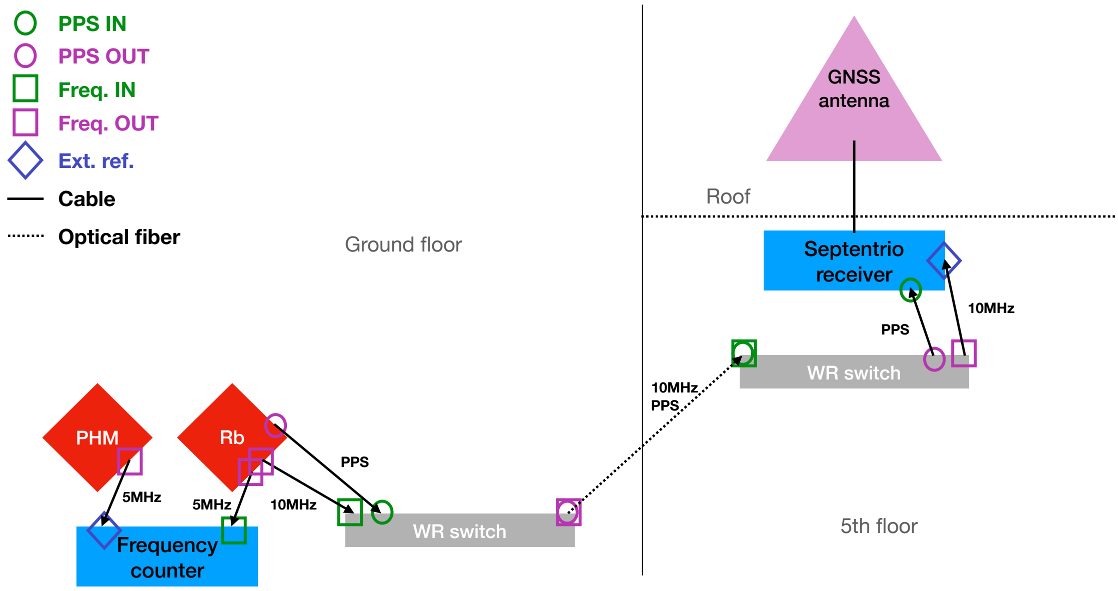

Figure 1. Experimental setup used in this work. Part of the equipment is installed at the ground floor and the other part at the fifth floor. The relevant signals generated at the ground floor are transported to the fifth floor via optical fibers with the White Rabbit (WR) protocol. This particular setup mimics what could happen in underground experiments where the clock signal would be generated underground whereas the GPS antenna and receiver would be located above-ground.

setup in Hyper-Kamiokande. It consists of a frequency counter measuring the frequency of the 5 MHz signal generated by the Rubidium clock. The reference for the internal clock of the counter is an external 5 MHz signal generated by a Passive Hydrogen Maser (PHM).

2.1.1 Rubidium clock

The Rubidium atomic clock used is the FS725 Rubidium Frequency Standard sold by Stanford Research Systems integrating a rubidium oscillator of the PRS10 model. It provides two 10 MHz and one 5 MHz signals with low phase white noise and its stability estimated via the Allan Standard Deviation (ASD) [17] at 1 s is about 2×10^{-11} (see Figure 2). It also provides a PPS output with a jitter of less than 1 ns. Its 20 years aging was estimated to less than 5×10^{-9} and the Mean Time Before Failure is over $200,000$ hours. It can also be frequency disciplined using an external 1 PPS reference, based on GPS for instance. The FS725 is installed at the ground floor of our laboratory and its 10 MHz and 1 PPS output are transported to the GNSS receiver at the fifth floor.

2.1.2 White Rabbit switches

The White Rabbit (WR) project [18] is a collaborative effort involving CERN, the GSI Helmholtz Centre for Heavy Ion Research, and other partners from academia and industry. Its primary objective is to develop a highly deterministic Ethernet-based network capable of achieving sub-nanosecond accuracy in time transfer. Initially, this network was implemented for distributing timing signals for control and data acquisition purposes at CERN's accelerator sites. The described experimental setup

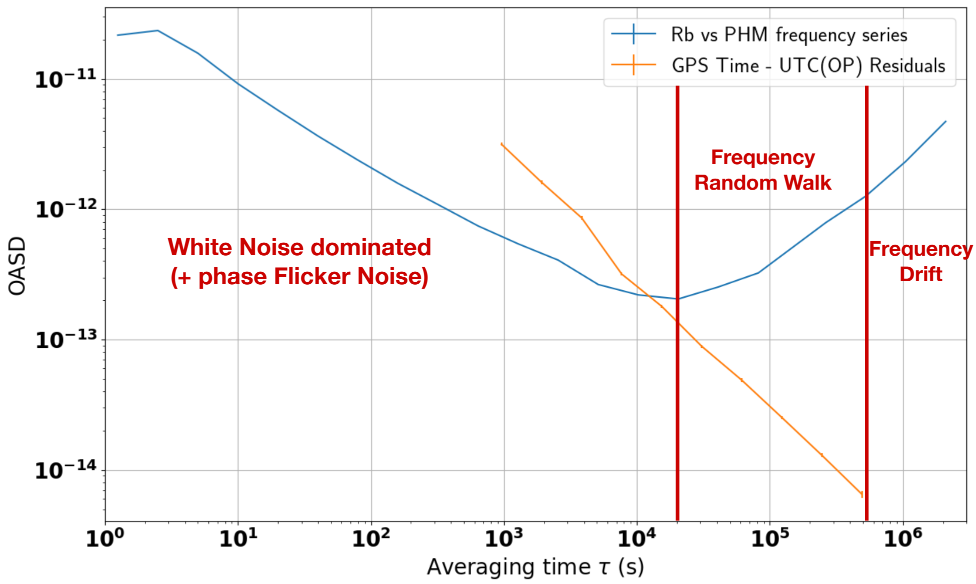

Figure 2. Overlapping Allan Standard Deviation of the Rb/PHM frequency ratio series (in blue), measured by the frequency counter before any correction, and of GPS Time vs UTC(OP) (in orange) measured by the Septentrio receiver. The main types of noises affecting the Rubidium clock stability are indicated where they are limiting the stability.

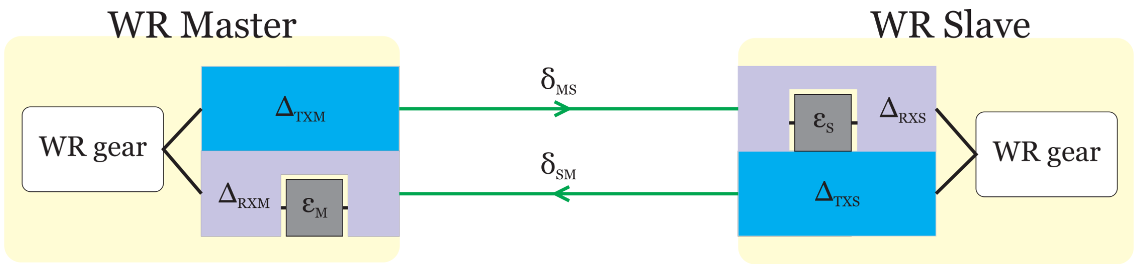

Figure 3. White Rabbit link model, from [19]

uses two WR switches to propagate with great precision the Rubidium clock PPS and frequency signals from the ground floor to the fifth floor.

The calibration of the link allows to obtain a sub-nanosecond synchronization between switches. A White Rabbit link between two devices is characterized by specific hardware delays and fiber propagation latencies. Each WR Master and WR Slave possesses fixed transmission and reception delays (ΔT_{XM}, ΔRXM, ΔT_{XS}, ΔRXS). These delays are the cumulative result of various factors such as SFP transceiver, PCB trace, electronic component delays, and internal FPGA chip delays. Additionally, there is a reception delay on both ends caused by aligning the recovered clock signal to the inter-symbol boundaries of the data stream, referred to as the bitslide value (ϵ_M and ϵ_S in Figure 3). We can see the results of calibration process using a counter in Figure 4, the difference of PPS signals between the WR slave and master switches changes from 165 ps to 60 ps (with a

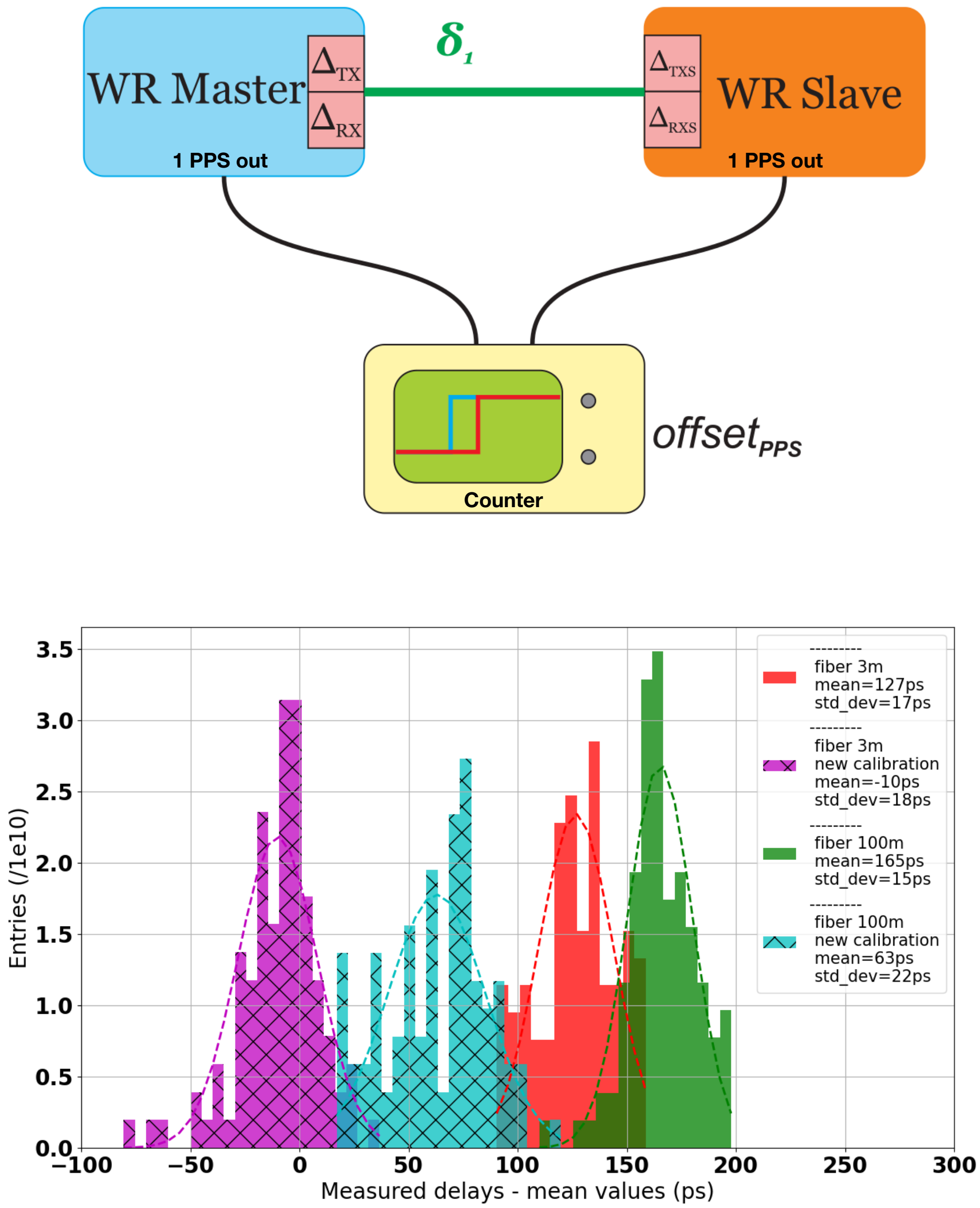

Figure 4. Difference between the PPS OUT signals of the White Rabbit slave and master switches before and after calibration

100 m long fiber). Delays introduced by the cables were subtracted to the mean values.

Note that the LPNHE, as a part of the T-REFIMEVE network [20, 21], has access through a dedicated switch to the official French realization of the UTC, called UTC(OP) (for Observatoire de Paris) [22], transported from the SYRTE laboratory via White Rabbit protocol. REFIMEVE is a French national research infrastructure aiming at the dissemination of highly accurate and stable time and frequency references to more than 30 research laboratories and research infrastructures all over France. The reference signals originate from LNE-SYRTE and are mainly transported over the optical fiber backbone of RENATER, the French National Research and Education Network. The UTC(OP) signal was not used in the final experimental setup because we do not foresee to have access to such a high precision signal in HK experiment. It was however used to characterize the GPS Time signal measured by the Septentrio receiver and whose OASD is shown in Figure 2.

2.1.3 Septentrio GPS antenna and receiver

We use the Septentrio PolaNt Choke ring GNSS antenna that supports GNSS signals from many satellite constellations including GPS, GLONASS, Galileo and BeiDou. In this work, we restrict the analysis to GPS but it can easily be generalized to any subset of constellations. The antenna position has been previously measured to a precision better than 6 mm by trilateration with the help of a web-based service provided by Canadian government [23]. We use a Septentrio PolaRx5 GNSS reference receiver as a timing receiver to compare GPS Time to the Rubidium clock. The receiver performs measurements based on the 10 MHz reference signal coming via White Rabbit from the Rubidium clock. The Rubidium clock 1 PPS signal is also transported to the receiver via White Rabbit to allow, at initialization, to identify the 10 MHz cycle. Note that this 1 PPS input is kept during the whole data-taking to avoid possible phase jumps due to perturbations. The Septentrio receiver provides one measurement every 16 min which is the middle point of the linear function fitted from the 13 min of data from the beginning of this 16 min time window. The results of the measurements are registered using the CGGTTS file format [24].

Before taking measurements, the whole system has been calibrated against official reference signals from the SYRTE laboratory. As it can be seen in Figure 5, the following delays need to be measured and taken into account during operation [25]. The calibration procedure [26] consists in measuring these:

- X_S: internal delay inside the antenna, frequency dependent
- X_C: delay caused by the antenna cable
- X_R: internal delay of the receiver for the antenna signal, frequency dependent
- X_P: in case an external signal is given in input, connection cable delay
- X_O: in case an external signal is given in input, internal receiver delay between external 1 PPS and internal clock

X_S and X_R depend on the GNSS carrier frequency that is being tracked, meaning it is specific to each frequency of each GNSS constellation. The calibration was performed for both GPS and Galileo constellations, each having two available carrier frequencies. The cable delays X_C and X_P were evaluated with an oscilloscope by sending a pulse in the cable and measuring the timing of the reflection. To reproduce the experimental conditions of underground experiments like HK or DUNE where the GPS antenna is outside, away from the detector, a 100 m cable was used and calibrated. The total cable delay was measured to be 505 ns. The internal delays of the antenna

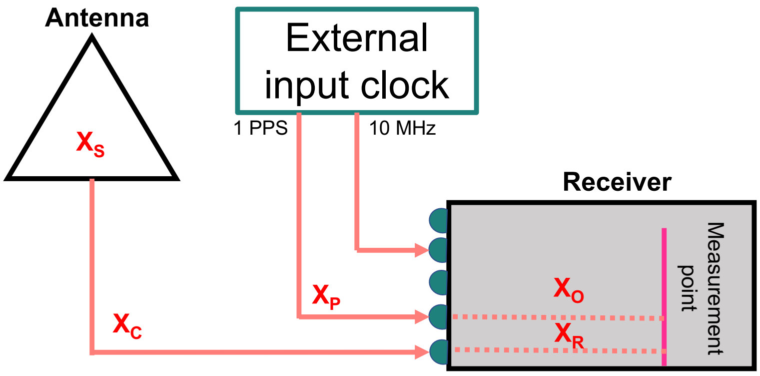

Figure 5. Delays to consider for the selected GNSS receiver+antenna pair, from [27]

and receiver can only be measured together (for each frequency) as INTDLY = $X_S + X_R$. This was done through a comparison with OP73, one of the calibrated GNSS stations of SYRTE, and with UTC(OP), the French realization of UTC, as an input to the two receivers. The values of INTDLY found for the two most widely available carrier frequencies of the GPS constellation (L1 and L2) and the Galileo constellation (E1 and E5a) are given in Table 1.

Table 1. Values of INTDLY in ns found for the first antenna+receiver system calibrated at the SYRTE lab against the OP73 station

GPS L1	GPS L2	Galileo E1	Galileo E5a
25.832	22.871	28.242	25.431

The delays X_C, INTDLY, and REFDLY can then be given as parameters of the receiver so that they are automatically handled in any further use of the receiver. Uncertainties on the measured delays were evaluated to 4 ns according to estimations fixed for the employed method. The calibration needs to be re-done for any new antenna+receiver+antenna cable combination.

2.1.4 Passive Hydrogen Maser

A Passive Hydrogen Maser (PHM) from T4 Science was also acquired. Note that this instrument is not available anymore. This atomic clock is approximately 10 times more expensive than a Rubidium clock but is also much more stable. Indeed, the Allan Standard Deviation (ASD), measured with our PHM in April 2022, was only of $\sim 3 \times 10^{-13}$ at 1 s and of 1.5×10^{-15} at 1 day. The PHM provides a 1 PPS signal as well as two outputs of 5 MHz, two outputs of 10 MHz, one output of 100 MHz and a sine output of 1 MHz as well as a 2.048 MHz square signal. Here, we use the PHM to generate a “perfect signal" to compare our Rubidium clock to.

2.1.5 Frequency counter

The frequency counter is the 53220A model from Keysight Technologies. It has two input channels and an input for an external frequency to use as a reference for its internal oscillator. The instrument can be used to measure the frequency of a signal input at any of the two channels. The instrument either uses directly its internal oscillator or, if specified by the user, the internal oscillator can be tuned to the external reference frequency. The external reference must be a sine wave with a frequency of 1, 5 or 10 MHz. The measurement resolution depends on the gate time corresponding to the integration time window: the longer the gate time, the better the resolution. The default resolution corresponds to a 0.1 s gate time.

The frequency counter was used in continuous mode to measure the Rubidium clock 5 MHz signal frequency simultaneously to the measurements performed by the Septentrio receiver. The external frequency reference was set to be the 5 MHz signal of the PHM and the resolution was set to 0.01 mHz which corresponds to a relative resolution of 2×10^{-11}. This resolution is good enough to measure the ASD of the Rubidium clock at low averaging times.

2.2 Corrections methods

2.2.1 General principle

To synchronize the Rubidium time stamps to UTC, we apply a time-dependent correction (quadratic or linear) to the time series generated by the free-running Rubidium clock $\phi_{Rb}(t)$. We model the k^{th} portion of the time series ($dt_{Rb,GPS}$), defined as the difference between the free-running Rb clock and the GPS Time, as a (one or two degrees) polynomial of time

$$\forall t \in [t_{k-1}, t_k], dt_{Rb,GPS}(t) = a_k \cdot t^2 + b_k \cdot t + c_k. \tag{2.1}$$

The coefficients a_k ($a_k = 0$ in case of linear fit), b_k and c_k of the polynomials are extracted from least square polynomial fits of the time difference distributions. The fits of these differences, obtained from the Septentrio receiver, are performed for every k^{th} time window of length Δt. In other words, we model the Septentrio measurements with a piece-wise polynomial function of time. For the k^{th} time window (between t_k and t_{k+1}), we get the corrected time stamps

$$\forall t \in [t_k, t_{k+1}],\ \phi_{Rb,corr}(t) = \phi_{Rb}(t) - a_k \times t^2 - b_k \times t - c_k. \tag{2.2}$$

The time-length Δt of the pieces (time windows) has to be chosen carefully. In particular, it should be short enough in order to correct for the effect of the frequency random walk of the Rubidium clock.

In the following, we consider two types of correction: the offline and the online corrections. The difference between the two methods is illustrated in Figure 6. The offline correction consists in using the Septentrio data from the same time-window as the Rubidium signal to extract the a_k, b_k and c_k coefficients. This correction is called offline because it requires the Septentrio data from up to $t_k + \Delta t = t_{k+1}$ to correct all the time stamps between t_k and t_{k+1} so it cannot be performed in real-time (one would need to wait a time Δt to extract the correction coefficients for the t_k time stamp).

The online correction consists in correcting the Rubidium time stamps between t_k and t_{k+1} using Septentrio data collected before t_k. One example of online correction is illustrated in Figure 6 where overlapping windows are used. This method is called online because it can be applied in real time. In the following, we will consider the most frequent possible update of the a_k, b_k and c_k coefficients: they will be updated every time we receive a new data point from the Septentrio

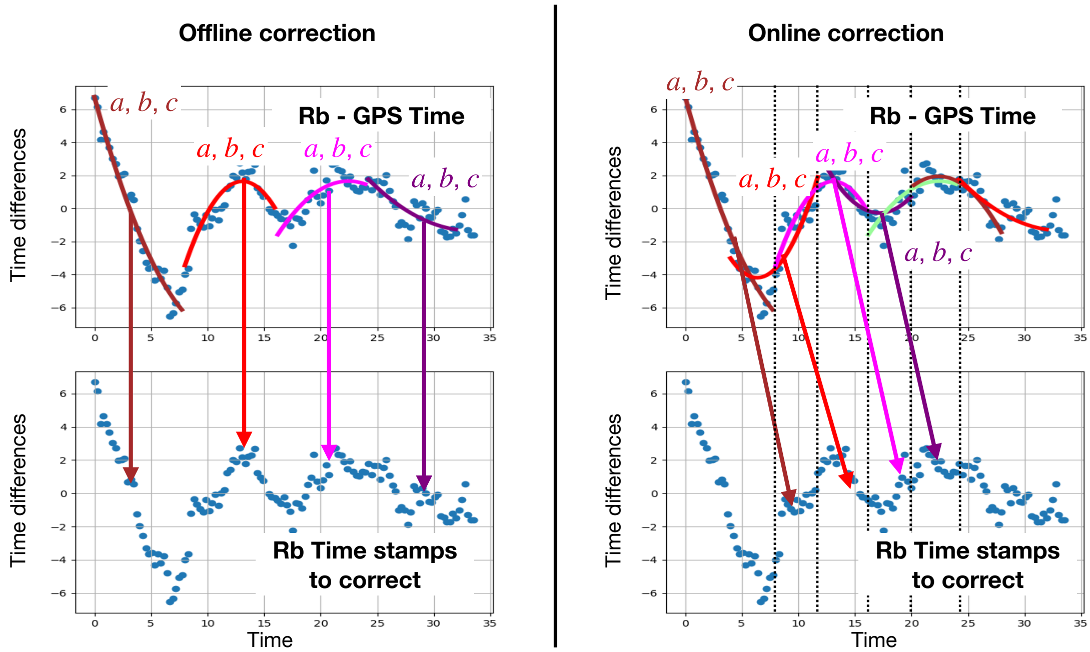

Figure 6. Schematic representation of the offline (left) and online (right) corrections. In the offline correction, we extract the correction coefficients using Rubidium - GPS Time comparison from the same time-window as the data we want to correct. In the online correction, we use Rubidium - GPS Time comparison from the previous time-window with respect to the data interval we want to correct. Only the second correction can be applied in real time as it only requires comparisons with GPS Time from previous measurements.

receiver (every $\delta t \approx 16$ minutes in our case). This means that we have $t_{k+1} = t_k + \delta t$ so that the a_k, b_k and c_k coefficients are extracted using Septentrio data between $t_k - \Delta t$ and t_k and are used to correct the time stamps between t_k and $t_k + \delta t$. In that particular case every Septentrio data point will have been used in multiple fits, the number depending on the length of the fit time window Δt.

The performance of the correction is evaluated in two ways. First, we look at the stability of the corrected time series estimated with the Overlapping Allan Standard Deviation (OASD). Then, we also look at the time difference against GPS signal after correction.

2.2.2 Validation of the method with simulations

Before evaluating the performance of our timing system when integrating the correction algorithm, the method was validated on simulated signals [27] in order to isolate the effect and performance of the correction from any measurement effect.

Simulation details Three types of signals were considered: a perfect clock to be used as a reference to evaluate the performance, a free-running Rubidium clock and a GPS time signal, as measured by the Septentrio receiver. The quadratic drift was not included because it is deterministic and therefore does not require further study for being corrected. At first order, the clock signal can be modeled by white noise (WN) in both phase and frequency as well as a random walk (RW) noise in frequency. Based on the characterization of the Rb clock, the phase and frequency flicker noises can be neglected for this purpose. Indeed, the characterization of our Rubidium clock in Figure 2 showed that the frequency flicker noise had a negligible impact on the OASD. Furthermore, the phase white and flicker noises have a similar impact on the standard OASD and cannot be distinguished here. We chose to ignore the phase flicker noise as it is less straightforward to simulate and it should not impact the long term random walk that we want to correct. The GPS Time can be modeled as pure phase white noise. The corresponding OASD as a function of the averaging time τ can be modeled [28–30] by:

$$OASD(\tau) \cong A_{WNp} \times \tau^{-1} + A_{WNf} \times \tau^{-1/2} + A_{RWf} \times \tau^{+1/2}. \tag{2.3}$$

The amplitudes A of these main frequency and phase noises were determined through fitting this model (Eq. 2.3) to the OASD of the data when characterizing our equipment (see Figure 2) and found to be:

$$\begin{aligned} A_{WNf} &= 7 \times 10^{-12}\ s^{1/2}, \\ A_{RWf} &= 1 \times 10^{-15}\ s^{-1/2}, \\ A_{WNp} &= 5 \times 10^{-11}\ s, \end{aligned} \tag{2.4}$$

for the free-running Rb clock and for the GPS Time:

$$\begin{aligned} A_{WNf} &= 0\ s^{1/2}, \\ A_{RWf} &= 0\ s^{-1/2}, \\ A_{WNp} &= 2 \times 10^{-9}\ s, \end{aligned} \tag{2.5}$$

with indices f and p for frequency and phase respectively. Using random numbers generation and a model with these types of noise discussed just above, time series were simulated.

The equivalent of 10^6 s of data was simulated. To mimic the output of the GNSS receiver, time differences between the simulated Rubidium clock and the simulated GPS Time (Δt^i_{Rb-ref}) are computed every 16 mn.

Offline corrections First, the offline corrections were tested on the simulated data. In Figure 7, the uncorrected simulated signals of the GPS and the clock are reported in dotted symbols for comparison. The increase of the clock's OASD after $\tau = 10^4$ s due to the random walk is clearly visible. One can see that the OASD of the corrected signals (starred symbols) do eliminate the random walk at longer terms which indicates a success of the correction method (quadratic). Moreover, one can determine that the ideal length Δt of the correction time windows lies around 3×10^4 s which corresponds logically to the intersection of the free-running Rb clock and GPS Time OASD curves. Indeed, the red curve with a time window of 28800 s shows an ideal combination of the short-term stability of the clock and the absence of random walk at longer scales. On the opposite, the yellow (shorter time window) and light blue (longer time window) curves show respectively a degradation of the short term performance and a remaining random walk component in the region between $\tau = 10^4$ s and the time window length (here 240000 s).

Online corrections The online (linear) correction method was then applied to the simulated data using time series directly and a correction window length of $\Delta t = 3 \times 10^4$ s. The results are shown in Figure 8 in red and prove to be just as efficient as the offline correction method to remove the random walk at longer time scales which is the main goal. The overall precision on the long term region (after $\approx 10^3$ s) is as expected slightly degraded compared to the offline correction.

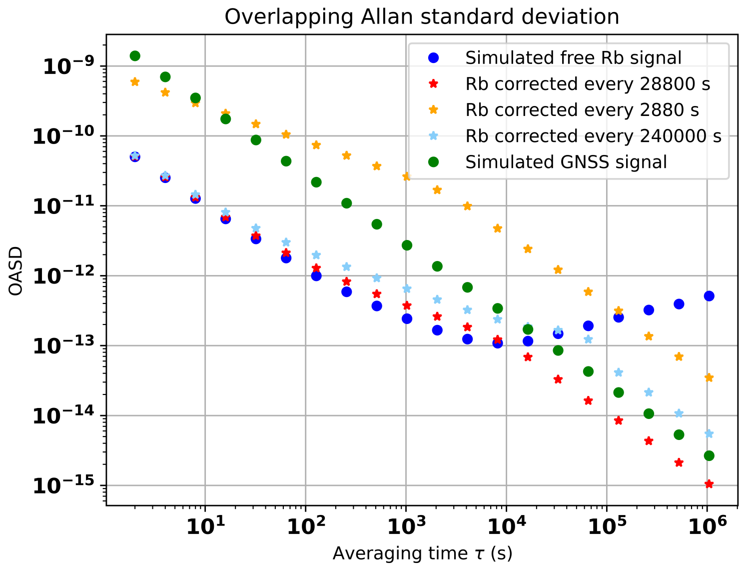

Figure 7. Comparison of overlapping ASD for corrected signals, with offline correction, with different time windows

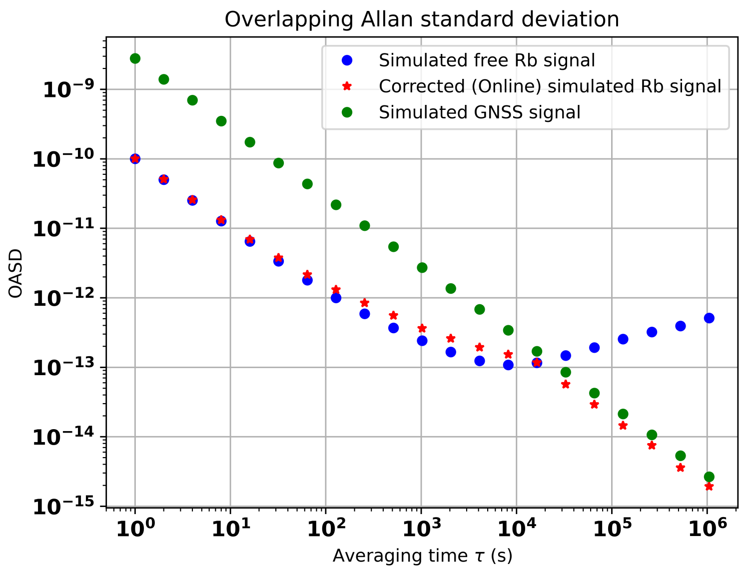

Figure 8. After online corrections at 3×10^4 s: Overlapping ASD with respect to perfect signal

Conclusion on simulation As a conclusion, it can be said that the application of the correction algorithms to the simulated signals allowed us to validate the chosen correction methods, both the offline and online ones. Indeed, looking at the residuals after correction in Figure 9, one can see that the remaining variations for both methods are well within the experimental requirements as they stay within a few ns. Seven different simulations were produced to take into account statistical fluctuations and the remaining time variations were found to be for offline and online corrections respectively $\sigma_{Off} = 0.64 \pm 0.06$ ns and $\sigma_{On} = 1.15 \pm 0.07$ ns.

Finally, it is important to note that although this validates the methods for application on data, those are simplified simulations, in particular because only the main noise types are taken into account. As a result, we do expect differences of performance of the correction on real data. It is also possible that the optimal time window for the correction is slightly different for real data because the simulations are not exact representation of data. Two main differences can be noted: the absence of frequency drift and flicker noises in the simulated Rubidium signal and the fact that we assume a perfect signal to compare the Rubidium signal to when evaluating the OASD.

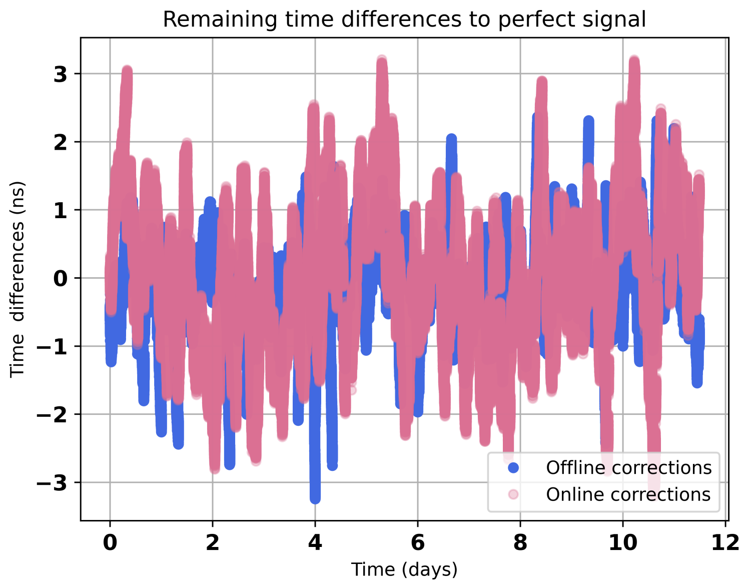

Figure 9. Comparison of time variations for simulated signals corrected with the offline method (blue) or with the sliding interval online method (pink)

2.2.3 Implementation on data

To check the impact of the correction we compare the Rubidium clock signal to that of another more stable clock, like a Passive Hydrogen Maser. The PHM signal plays the role of the perfect signal used for the simulations, while obviously not being perfect. This first difference is to take into account while comparing performances on simulated data to performance on experimental data. In the following, we will also quantify the stability of the Rubidium signal using the OASD of a series of frequency ratios (according to equation (10) of [31]) between this signal and the 5 MHz generated by the PHM. Measuring this ratio frequently, once per second for instance, would allow to also evaluate the very short term stability of the corrected signal which is not possible with the Septentrio measurements that are integrated over 16 minutes. We use the frequency counter to provide a measurement per second of the Rubidium clock 5 MHz frequency f^i_{Rb} taking the PHM 5 MHz generated signal as a frequency reference f_{ref}. We then perform a simultaneous correction of the Rubidium - GPS Time, as measured by the Septentrio receiver, and of this frequency ratio $f^i = f_{Rb}/f_{ref}$ series. Comparing the OASD of the corrected frequency series to the uncorrected one, one can quantify the short term stability (below 16 minutes) after correction while making sure that the random walk was corrected. We can also use this comparison to optimize the value of Δt in order to achieve the lowest Allan Standard Deviation possible at all averaging time windows.

3 Results

In this Section, we present the results of the correction of the Rubidium clock time stamps obtained for simultaneous measurements of $\sim$ 50 days with the Septentrio receiver and the frequency counter with PHM 5 MHz signal as a frequency reference. The frequency measurements are divided by the expected value to obtain a series of Rb/PHM frequency ratios. The OASD of such a frequency series is shown in Figure 2. Note that the statistical uncertainty on the estimated OASD, due to the limited number of samples per averaging time, are included as error bars for both curves (Rb and GPS) but they are too small to be visible. Indeed for the Rb vs PHM OASD, the statistical uncertainty is at the permil level. Up to an averaging time of around 10^4 s, the stability is limited only by the phase white noise and then by the frequency white noise. After that, the OASD first increases as $\tau^{1/2}$ which is characteristic of the frequency random walk. From $\tau \approx 5 \times 10^5$ s, the OASD increases proportionally to τ. This is characteristic of a deterministic frequency drift which can be easily characterized and corrected for contrary to the frequency random walk. In comparison, the OASD of the difference between GPS Time and UTC(OP) that we receive from the SYRTE laboratory via White Rabbit network, is only limited by a phase white noise at least up to an averaging time of 5×10^5 s: the OASD keeps decreasing with the averaging time. At low averaging times, the GPS stability is worse than that of the Rb because of this phase white noise: the GPS OASD is of around 3×10^{-12} at 960 s compared to around 7×10^{-13} OASD for the Rubidium clock. However, at around 10^4 s, the stability of the Rb signal becomes worse compared to GPS Time because of the frequency random walk and drift of the Rubidium clock.

In this paper, we used only the GPS satellites with an elevation angle (angle between line of sight and horizontal direction) larger than 15° to extract the Rubidium time residuals distribution. During the whole data-taking period, for each data point, the Septentrio receiver was able to track an average of 6.5 GPS satellites and at least 4 GPS satellites for each data point. To obtain the Rubidium vs GPS Time difference, we take the mean value of the differences between the Rubidium clock and each GPS satellite tracked in the same integration time window of the Septentrio receiver. The obtained time difference is shown in Figure 10. The time difference shown here have already been corrected for the deterministic drift discussed before as this can be easily monitored and corrected for contrarily to the random walk. To correct for both this frequency drift, we performed a quadratic fit of the first few days of Septentrio measurements and subtracted the results to the Septentrio data. The frequency drift was measured at around 10^{-18} s^{-1} which would induce a drift of 100 ns after less than four days. Note that the correction of the frequency deterministic drift could be actualized regularly with new fits of the time difference over a long enough period (a few days of data) but it was not found to be necessary for our example with 50 days of data-taking. In the following, the same initial correction of the frequency drift was applied to the Rb vs PHM data. The correction coefficients will be extracted from the residual time difference. Before correction, we see that after a few days of data-taking, the Rb clock can drift away from the GPS Time by more than a hundred nanoseconds because of the random walk noise.

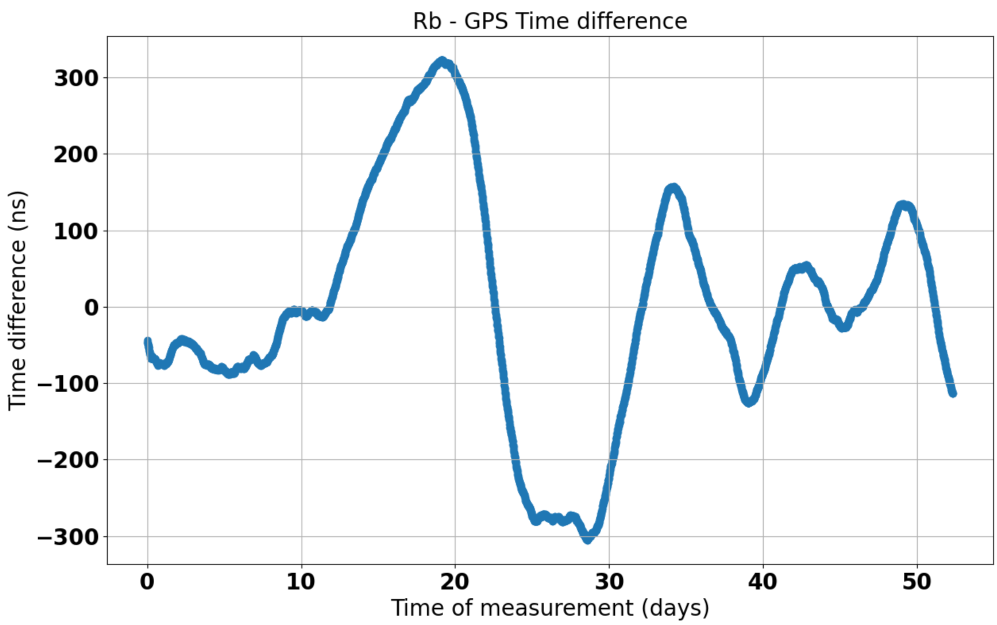

Figure 10. Time difference between the Rubidium clock and GPS Time as measured by the Septentrio receiver. The data are already corrected for the deterministic drift of the Rubidium clock. The large variations are caused by the frequency random walk of the Rubidium clock.

3.1 Offline correction

Figure 11 shows the Allan Standard Deviation of the Rubidium vs PHM data. Note that a relative resolution of 10^{-11} was chosen for the frequency measurement with the frequency counter. This is lower than the Phase White Noise of the free-running Rubidium clock so it does not impact significantly the Allan Standard Deviation. The blue curve shows the result for series corrected only for the deterministic drift of the Rubidium clock, by subtracting the expected time distribution of the series caused by this drift. Note that by correcting the deterministic drift, we also partially correct for the frequency random walk such that the OASD decreases with the averaging times for $\tau > 10^6$ s. The other colored curves show the results for the series corrected offline, with different width of the correction time window. Here, we use quadratic fits of the Septentrio data (so $a_k \neq 0$ a priori). The frequency series were integrated to obtain time series to which we subtracted the fit results. The shortest time window (2880 s) corresponds to approximately 3 Septentrio 16 minutes epochs. The medium (10560 s) and largest (240,000 s) correspond respectively to 11 and 250 Septentrio data points.

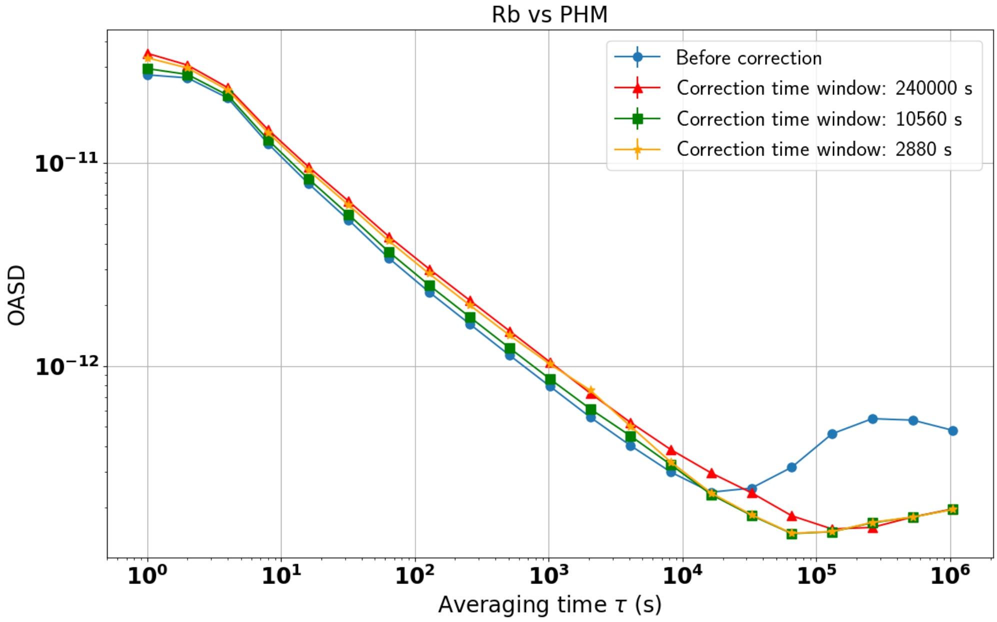

Figure 11. Overlapping Allan Standard Deviation of the Rb/PHM frequency ratios series after the deterministic drift correction (in blue) and after the correction with a correction time window of 2880 s (orange), 10560 s (green) and 240, 000 s (red). The best stability at both short and long averaging times is obtained for the medium time window (10560 s≈ 3 hours).

One sees that with the medium time window compared to the two others, we obtain the best stability at all averaging times. At lower averaging times, the performance is very similar to the uncorrected time series. At higher averaging times, the Allan Standard Deviation is much better than the uncorrected series and is comparable to the one obtained for the shortest correction time window. This illustrates the fact that both the 2880 s and 10560 s windows are able to correct very well the frequency random walk ($\tau^{1/2}$ component of the ASD) of the uncorrected time series. However, with the shortest correction time window, the short term stability of the time series is degraded compared to the uncorrected series: the value of the ASD at 1 s increases by a factor ~ 1.5. In this scenario, the corrected Rubidium time signal gets very close to GPS Time which is known to have a higher phase White Noise. Finally, the longest correction time window leads to a similar stability as the shortest one at long term, and even poorer stability at $\tau \in [10^4, 10^5]$ s.

Figure 12 shows the Rubidium vs GPS Time difference after the offline correction. The shorter the correction time window, the better. However, with the medium length time window, we still get time residuals lower than 5 ns over the whole data-taking period, which is well below the requirements of HK. With the longest correction time window, jumps of a few tens of nanoseconds are introduced in the time residuals. This explains the overall higher ASD: the stability of the signal is limited by those jumps. These jumps can be understood by looking at the fit of the Septentrio data in this scenario in Figure 13. The time scale of the variations in the data to fit is too small compared to the 240, 000 s time window. In consequence, the fitted tendency from one piece to another is very different, and the fitted piece-wise polynomial is not continuous.

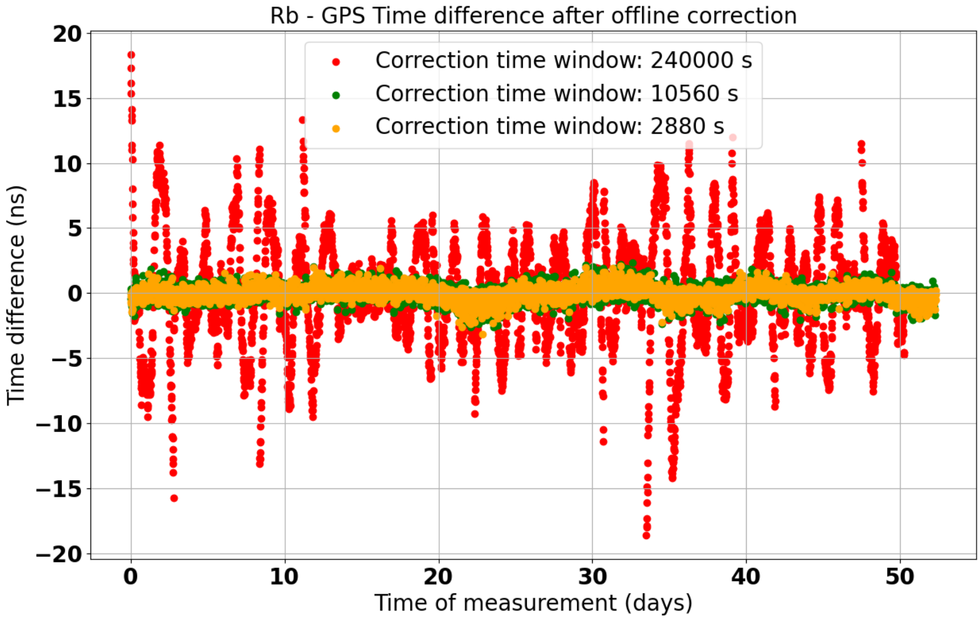

Figure 12. Time difference between the Rubidium clock and GPS Time after the offline correction. Three different correction time windows have been tested: 2800 s (orange), 10560 s (green) and $240,000$ s (red). These residuals can be compared to the residuals before correction that were shown in Figure 10.

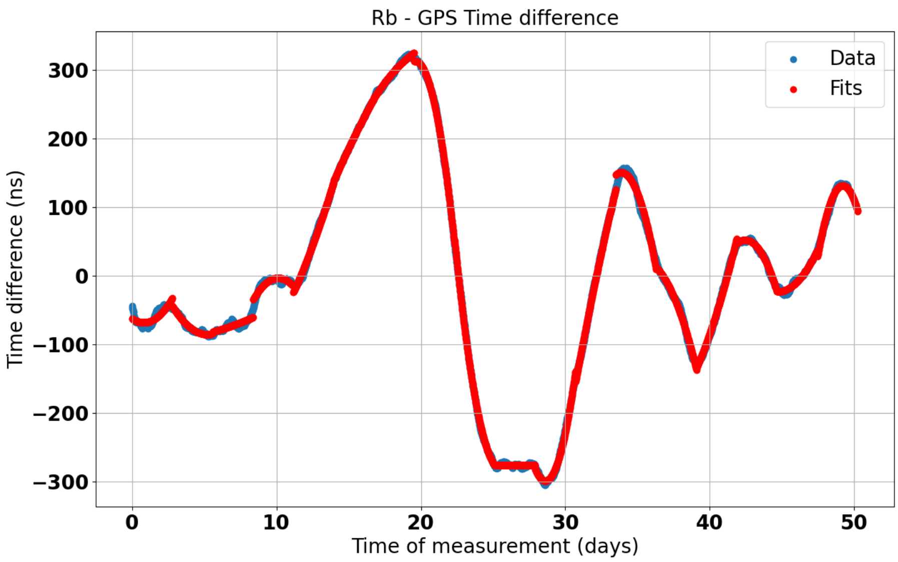

Figure 13. Time difference between the Rubidium clock and GPS Time. The red portions show the results of the polynomial fit over consecutive time windows of $240,000$ s. The fit sometimes fail to represent the shorter time scales variations of the measured data. The poor fit quality can then lead to introducing jumps in the corrected time signal.

With the offline version of the corrections, we thus obtain a very good synchronization to GPS Time at the level of a few nanoseconds with the 10560 s time window. However, this version of the correction cannot be applied in real time. In the following paragraphs, we show the results for the online version of the correction that can be applied in real time to correct the time stamps of events in physics experiments.

3.2 Online correction

Figure 14 shows the Allan Standard Deviation of the uncorrected (blue) and online corrected (other colors) Rubidium vs PHM frequency times series. The same three time window intervals as in the offline correction scenario are considered. The top panel shows the results using quadratic fits of the Septentrio data and the bottom panel shows the results with linear fits. For the shortest and medium correction time windows, the linear fits lead to better performance with a lower OASD at low averaging times. At 1 s, the OASD with the shortest (medium) correction time window is reduced by a factor 4 (resp. ~ 1.5).

This behavior is very understandable looking at the number of degrees of freedom (number of data points - number of free parameters) in our fits. For the shortest time windows, the number of degrees of freedom is relatively low (0 and 8) in case of quadratic fits so we risk over-fitting to the past data in order to correct the present data. This number of degrees of freedom is less relevant in the offline correction as the fit is performed on the same data as the correction (the over-fitting is not a problem here). Lowering the number of free parameters is one way of increasing the degrees of freedom hence allowing the fit to better generalize to the present data. Another way to increase the number of degrees of freedom is to increase the number of data points in the fit. For the longest time window, there are 247 degrees of freedom in the quadratic fit so we lower the risk of over-fitting. On the contrary, in that case, quadratic fits lead to a slightly better correction of the random walk that limits the stability only up to $\tau \approx 8 \times 10^4$ s whereas with linear fits, it limits the stability up to $\approx 2 \times 10^5$ s. Here, Figure 14 shows a clear degradation of the stability after correction for averaging times lower than the correction window's length. This is a known effect from linear servo loop theories and periodic perturbations of oscillators [32] and it could be attenuated by scaling down the correction: instead of subtracting the result of the fit, we could subtract only a fraction of it. Additionally, degradation of short term stability because of over-fitting on data from the past is, also visible in the OASD of the Rb vs GPS time difference after correction shown in Figure 15. This plot also illustrates that the corrected series stability, compared to GPS Time, is not limited by any frequency random walk at least up to an averaging time of 2×10^6 s and with a correction time window short enough. Indeed, in that case, the OASD keeps decreasing with increasing averaging time.

Regarding the stability of the corrected Rubidium clock, using linear fits, the conclusions are the same as for the offline correction. The lowest Allan Standard Deviation, for all averaging times, is achieved with the medium width correction time window. With the shortest time window, the short term stability is degraded, whereas it is the long term stability that is degraded (compared to the other corrected scenarios) with the longest correction time window. Note that, contrary to the offline correction, the online correction with very long time windows does not deteriorate the short term stability. This is due to the use of "overlapping" windows of Rb vs GPS data. Between two consecutive fits, there is only one data point out of the 250 used that changes (the oldest one from

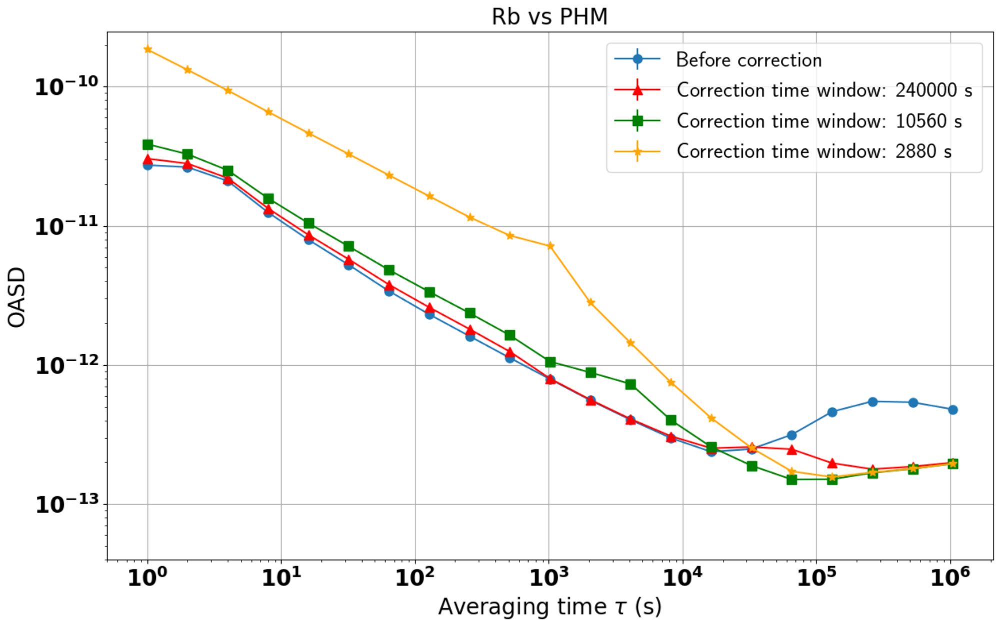

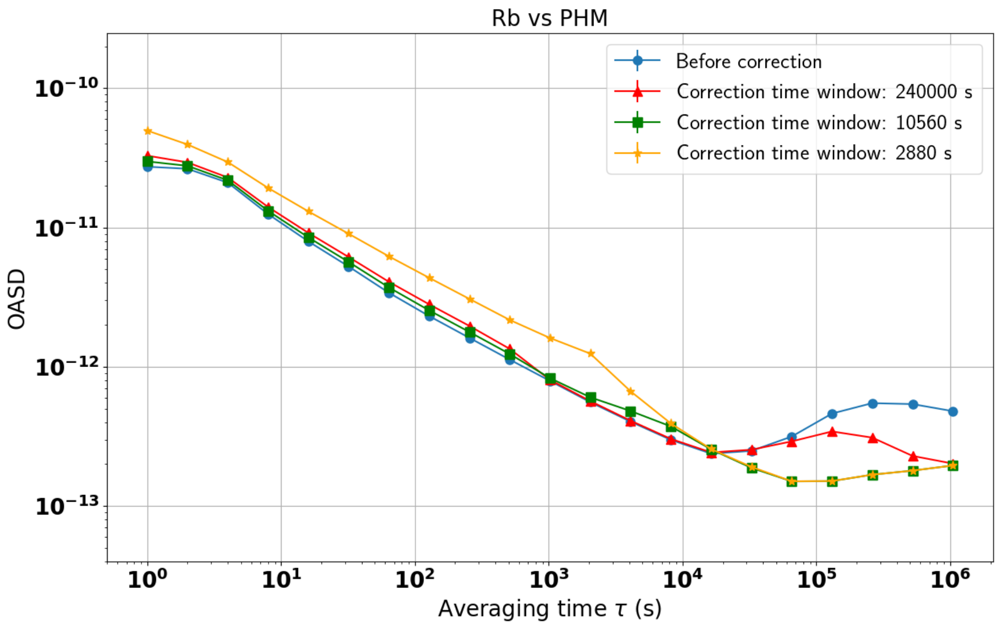

Figure 14. Overlapping Allan Standard Deviation of the Rb/PHM frequency ratios series after the deterministic drift correction (in blue) and after the online correction with a correction time window of 2880 s (orange), 10560 s (green) and 240,000 s (red). The data were fitted with quadratic (top) or linear (bottom) functions of time. A better stability, similar to the offline correction, can be obtained using linear fits.

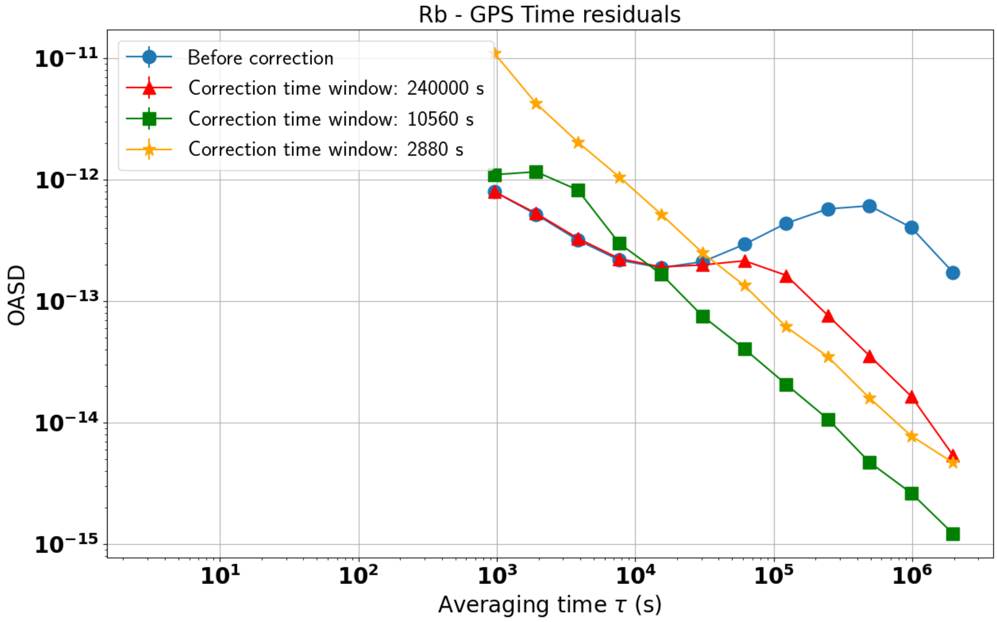

Figure 15. Overlapping Allan Standard Deviation of the Rb vs GPS Time residuals series after the deterministic drift correction (in blue) and after the online correction with a correction time window of 2880 s (orange), 10560 s (green) and 240, 000 s (red). Note that before the deterministic drift correction, the OASD of this signal is the combination of the GPS Time OASD at low τ and the Rubidium OASD at high τ, i.e: the combination of the blue and orange curves of Figure 2. The deterministic drift correction slightly smooths the residuals so that the OASD becomes generally lower and the frequency drift and random walk at high τ disappears, hence the decreasing OASD in the blue curve at very high τ. The time residuals were fitted with quadratic functions of time. The increase of OASD at 1 s averaging time with decreasing correction time window is consistent with what is observed in the Rb/PHM frequency ratios series after online correction. The less degrees of freedom in the fit, the more we risk over-fitting on past data and lowering the short term stability of the signal.

the previous fit is replaced by the newest point). The fit parameters cannot change too abruptly from one fit to another so the resulting distributions are smooth.

If the correction time window is too wide, we cannot correct as well the frequency random walk of the free-running Rubidium: the risk is that the Rubidium time signal locally drifts too far away from the GPS Time. This can be observed in the corrected Rubidium against GPS Time in Figure 16 where the maximum difference reaches $\sim$ 60 ns (or $\sim$ 25 ns with quadratic fits) with the 240, 000 s correction time window. With the 10560 s correction time window, the differences stay in the $\pm$5 ns range. Once again, one can see the reduction of the white noise when using linear instead of quadratic fits for the 2880 s correction time window scenario: the residuals are contained in a $\pm$5 ns range with linear fits instead of $\pm$12 ns with quadratic fits. Before correction, as the reader saw in Figure 10, the free-running Rubidium clock can drift by around 100 ns in 10 days which means that HK's requirement for the synchronization with UTC is not met. After online correction with the longest time window tested, the corrected Rubidium time stamps drift by around 60 ns in

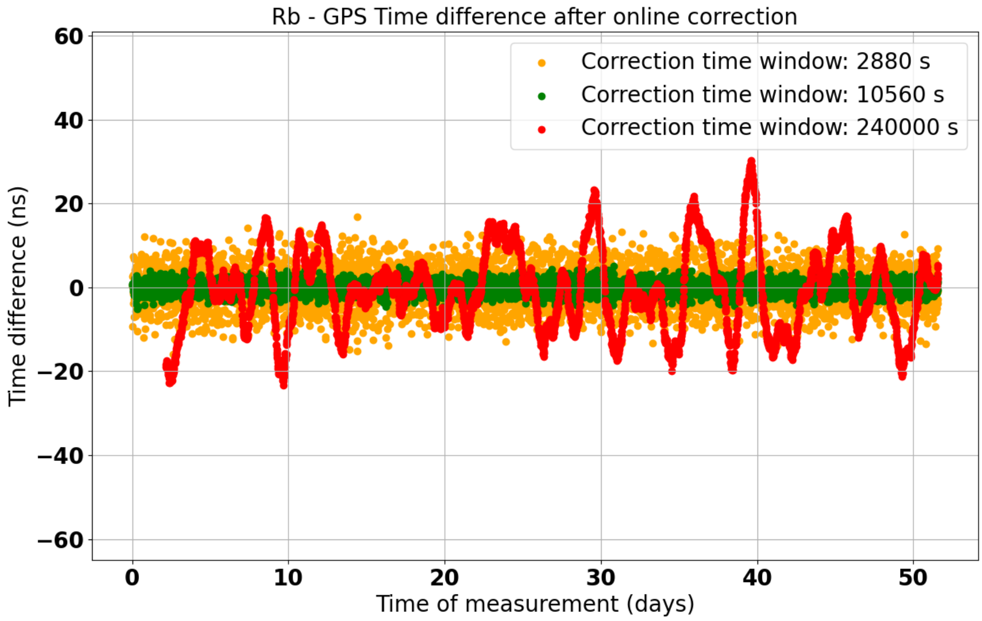

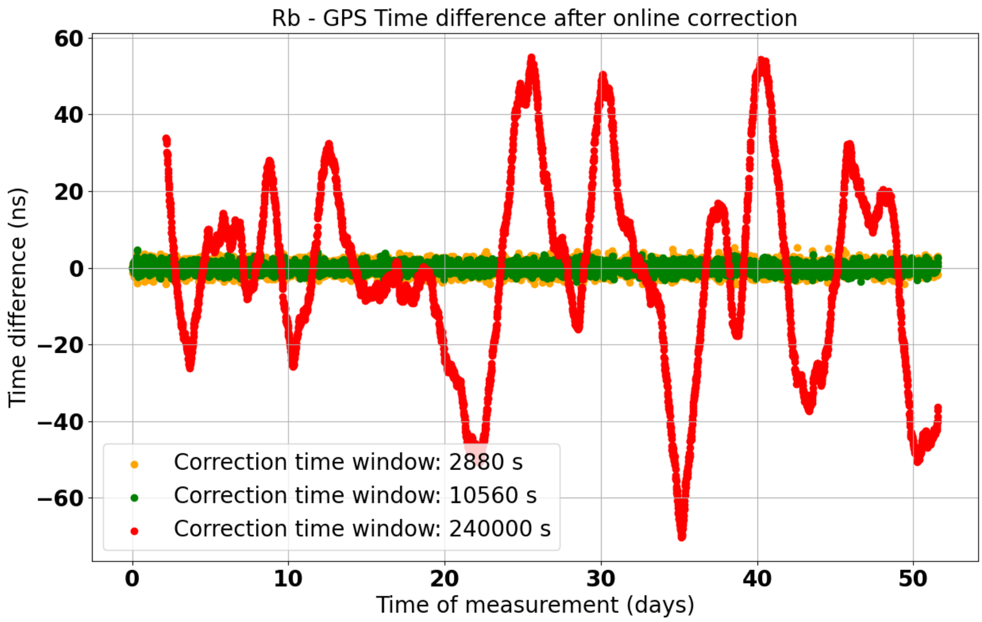

Figure 16. Time difference between the Rubidium clock and GPS Time after the online correction. Each point is corrected using a quadratic (top) or linear (bottom) fit of the 2800 s (orange) or 10560 s (green) or 240, 000 s (red) of data points prior to this point. Using linear fits leads to smaller residuals for the shortest time window and bigger ones for the longest time window.

a few days because of remaining random walk noise. Even though during the 50 days data-taking period the time residuals with respect to GPS Time does not exceed 100 ns, it is not possible to safely claim that the Rubidium clock drift will not exceed HK's requirement of 100 ns if we use the 240, 000 s correction time window. With shorter time windows, this drift seems to be dominated by white noise and is thus contained in a range of a few nanoseconds.

4 Discussion

As advertised before, the advantage of the so-called online correction is that it could be performed in real-time. This is an important feature for applications that necessitate a real-time synchronization with UTC or with another site (like the future HK or DUNE experiments). If a reference clock signal is generated with an atomic clock (like the Rubidium clock used here) and sent to a data acquisition system to be propagated to detectors and provide time stamps, one could continuously compare this signal to GPS Time using a Septentrio receiver. The correction coefficients a, b and c calculated from the Septentrio data would need to be sent to the data acquisition system so that it could correct the time stamps in real-time.

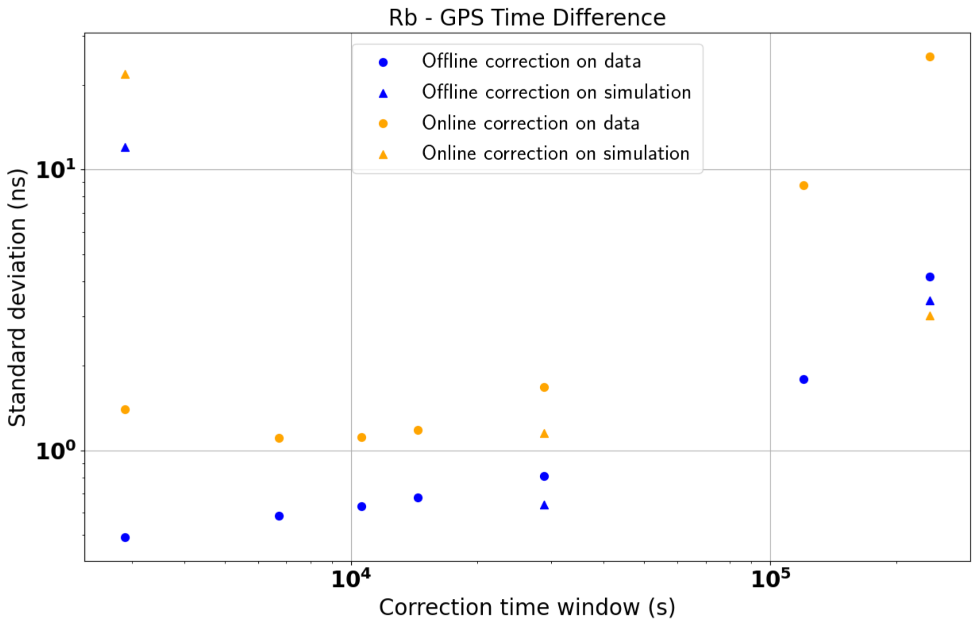

Figure 17. Standard deviation of the residuals distributions between the Rb and the GPS Time after the offline (blue) or online (orange) correction as a function of the correction time window. Quadratic fits of the Septentrio data are used for the offline correction whereas linear fits are used for the online correction. The performance on simulated data is also shown for the 10560 s time window with triangle markers.

Figure 17 shows the standard deviation of the Rb vs GPS Time difference after correction as a function of the correction time window's width. The performance of the offline and online corrections on experimental data (colored dots) are compared to the performance we had obtained on simulated data (colored triangles) with a correction time window of 2880 s, 28800 s and

240000 s. Note that these simulated data were only taking into account phase white noise, frequency white noise and frequency random walk components. No additional uncertainties were added to take into account other types of noise (e.g: flicker noise) or experimental conditions (e.g: imperfect calibrations, imperfect PHM time signal). These differences can explain the slightly better achievable performance obtained on simulated data (0.64-1.15 ns at $28,800$ s) compared to experimental data (0.81-1.67 ns at $28,800$ s) and the fact that the residuals are minimal with a time window of $28,800$ s with simulated data and $10,560$ s with experimental data. For both corrections, very similar performance of synchronization with GPS Time are obtained for correction time windows below $30,000$ s so there is no need to have much shorter windows. This result is consistent with the fact that, as seen in Figure 2, the stability of the Rubidium signal becomes limited by the frequency random walk for averaging times around 10^4 s. It is also for similar averaging time windows that the Rubidium clock stability becomes worse than that of GPS Time. It was thus expected to find that similar correction time windows or shorter ones would be needed to efficiently correct for the random walk. The offline correction seems to provide a slightly better synchronization to GPS Time (down to ~ 1 ns) but the precision achievable with the online correction is already more than satisfying (better than 5 ns for correction time windows below $100,000$ s) for synchronization between several experimental sites. Indeed, the needed level of synchronization is usually of the order of 100 ns for those applications.

Note that the algorithms presented here were optimized to correct time stamps, provided by a free-running Rubidium clock, that were already corrected to eliminate the impact of the Rubidium clock frequency linear drift. This initial correction was done here once and for all by fitting the first few days of the time difference with respect to the GPS Time. This was found to be enough for a data-taking of around 50 days. However, for a longer data-taking, one could regularly update this preliminary correction by fitting again the last few days of Septentrio data and subtracting the fit result before moving to the fit with shorter time windows (typically $10,560$ s) dedicated to the random walk correction.

5 Conclusions

In this paper, we presented a simple way to use time comparisons to GPS Time to synchronize the time stamps, generated using a free-running Rubidium clock, close to UTC while preserving its short term stability and correcting the long term frequency random walk. This method has the advantage of using relatively cheap instruments and to be applicable online for a real-time synchronization as well as to be robust against GPS signal reception failures. The online method could be applied for the real-time synchronization between several experimental sites in long-baseline neutrino physics experiments.

This method consists in fitting the GPS Time vs Rb measured by a GNSS receiver with a piece-wise polynomial function of time and in subtracting the result to the generated time stamps. The method was first designed and validated with simulated signals before assessing its performance on real data. We evaluated the performance of this correction by quantifying the stability of the clock signal before and after the correction using the Overlapping Allan Standard Deviation. We showed that the optimal length of the time window for the fit of the GPS Time vs Rb seats around $10,000$ seconds, corresponding to 11 data points from the receiver. This time window allowed to maintain the best possible short term stability while correcting efficiently the frequency random walk. After correction with this time window, the difference to GPS Time stays within a window of ±3.5 ns (±5 ns) for the offline (resp. online) correction during the whole period of ∼ 50 days of measurement. This performance largely meets the usual requirements for long-baseline neutrino physics experiments, like Hyper-Kamiokande and DUNE. Note that we do not expect the performance of the correction to be heavily degraded by isolated missing or outlier measurements from the receiver. However, this correction requires a constant monitoring of the Rubidium time signal with a GNSS receiver (or other reference that can be linked to UTC). One should thus make sure that such a reference is available in the long term and that there is no possibility to loose it for long periods (e.g.: several hours).

Acknowledgments

This research was funded by IN2P3/CNRS, the French "Agence nationale pour la recherche" under grant number ANR-21-CE31-0008, the "IdEx Sorbonne Université" and the 2019 "Sorbonne Université Émergences: MULTIPLY" grant.

The White Rabbit network and the access of associated optical fibers to the Pierre and Marie Curie campus: T-REFIMEVE, FIRST TF and LNE: "Agence Nationale de la Recherche" (ANR-21-ESRE-0029 / ESR/Equipex T-REFIMEVE, ANR-10-LABX48-01 / Labex First-TF); Laboratoire National d’Essai (LNE), project TORTUE.

References

[1] M. Guler et al., *OPERA: An appearance experiment to search for nu/mu <–> nu/tau oscillations in the CNGS beam*, Experimental proposal, CERN-SPSC-2000-028.

[2] K. Abe et al., T2K Collaboration, *The T2K Experiment*, *Nucl. Instrum. Meth. A* **659** (2011), 106-135, doi:10.1016/j.nima.2011.06.067, arXiv:1106.1238.

[3] D. S. Ayres et al., *The NOvA Technical Design Report*, (2007), doi:10.2172/935497.

[4] K. Abe et al., *Hyper-Kamiokande Proto-Collaboration, Hyper-Kamiokande Design Report*, (2018), arXiv:1805.04163.

[5] B. Abi et al., *Deep Underground Neutrino Experiment (DUNE), Far Detector Technical Design Report, Volume I: Introduction to DUNE*, (2020), arXiv:2002.02967.

[6] D. Cussans et al., *Timing and synchronization of the DUNE neutrino detector*, *Nuclear Instruments and Methods in Physics Research, A* **958** (2020), doi:10.1016/j.nima.2019.04.097.

[7] P. Mészáros, D.B. Fox, C. Hanna et al., *Multi-messenger astrophysics*, *Nat. Rev. Phys.* **1** (2019) 585–599, https://doi.org/10.1038/s42254-019-0101-z.

[8] The Supernova Early Warning System web page, https://snews2.org/.

[9] K. Abe et al., T2K collaboration, *Upper bound on neutrino mass based on T2K neutrino timing measurements*, *Physical Review D* **93** (2016) 1, 012006, DOI: 10.1103/PhysRevD.93.012006, https://arxiv.org/abs/1502.06605.

[10] Y. Fukuda et al., Super-Kamiokande collaboration, *The Super-Kamiokande detector*, *Nucl.Instrum.Meth.A* **501** (2003) 418, https://doi.org/10.1016/S0168-9002(03)00425-X.

[11] L. Mellet, M. Guigue, B. Popov, S. Russo, V. Voisin, on behalf of the Hyper-Kamiokande Collaboration, *Development of a Clock Generation and Time Distribution System for Hyper-Kamiokande*, *Phys. Sci. Forum* **8** (2023) 72, https://doi.org/10.3390/psf2023008072.

[12] M. Lombardi, *Fundamentals of Time and Frequency*, *The Mechatronics Handbook*, CRC Press: Boca Raton, FL, USA (2002), ISBN 978-0-8493-6358-0.

[13] Giulia Brunetti, *Neutrino velocity measurement with the OPERA experiment in the CNGS beam*, Université Claude Bernard - Lyon I; Università degli studi (Bologne, Italie), 2011. English. ⟨NNT : 2011LYO10088⟩. ⟨tel-00843100⟩

[14] M.A. Weiss, G. Petit, Z. Jiang, *A comparison of GPS common-view time transfer to all-in-view*, In Proceedings of the *IEEE International Frequency Control Symposium and Exposition*, 2005.

[15] The National Institute of Information and Communications Technology (NICT), Japan. https://www.nict.go.jp/en/

[16] https://www.bipm.org/en/time-ftp/circular-t

[17] D.A. Howe, D.W. Allan, J.A. Barnes, *Properties of signal sources and measurement methods*, In Proceedings of the Thirty Fifth Annual Frequency Control Symposium, Philadelphia, USA, 27-29 May 1981.

[18] J. Serrano et al., *The White Rabbit project* (2013), https://cds.cern.ch/record/1743073.

[19] G. Daniluk, *White Rabbit calibration procedure (version 1.1)* (2015), https://white-rabbit.web.cern.ch/documents/WR_Calibration-v1.1-20151109.pdf

[20] E. Cantin et al., *REFIMEVE Fiber Network for Time and Frequency Dissemination and Applications*, 2023 Joint Conference of the European Frequency and Time Forum and IEEE International Frequency Control Symposium (EFTF/IFCS), Toyama, Japan, 2023, pp. 1-4, doi: 10.1109/EFTF/IFCS57587.2023.10272084.

[21] C. B. Lim et al., *Extension of REFIMEVE with a White Rabbit Network*, 2023 Joint Conference of the European Frequency and Time Forum and IEEE International Frequency Control Symposium (EFTF/IFCS), Toyama, Japan, 2023, pp. 1-4, doi: 10.1109/EFTF/IFCS57587.2023.10272069.

[22] G. D. Rovera et al., *UTC(OP) based on LNE-SYRTE atomic fountain primary frequency standards*, *Metrologia* **53** (2016) S81.

[23] https://webapp.csrs-scrs.nrcan-rncan.gc.ca/geod/tools-outils/ppp.php

[24] P. Defraigne, G. Petit, *CGGTTS-Version 2E: an extended standard for GPS Time Transfer*, *Metrologia* **52** (2015), IOP Publishing, DOI: 10.1088/0026-1394/52/6/G1.

[25] J. Plumb et al., *Absolute calibration of a geodetic time transfer system*, *Ultrasonics, Ferroelectrics and Frequency Control, IEEE Transactions* **52** (2005) 1904-1911, doi = 10.1109/TUFFC.2005.1561658.

[26] G. D. Rovera et al., *Link calibration against receiver calibration time transfer uncertainty when using the Global Positioning System*, *Metrologia* **51.5** 476490 (2014).

[27] Lucile Mellet, *From T2K to Hyper-Kamiokande : neutrino oscillation analysis and preparation of the time synchronization system*, PhD thesis, Sorbonne University (2023), ⟨NNT : 2023SORUS297⟩ ⟨tel-04284182⟩.

[28] J. A. Barnes et al., *Characterization of Frequency Stability*, in *IEEE Transactions on Instrumentation and Measurement*, vol. IM-20, no. 2, pp. 105-120, May 1971, doi: 10.1109/TIM.1971.5570702.

[29] T. J. Witt, *Using the Allan variance and power spectral density to characterize DC nanovoltmeters*, in *IEEE* Transactions on Instrumentation and Measurement, vol. 50, no. 2, pp. 445-448, April 2001, doi: 10.1109/19.918162.

[30] D. W. Allan, *Statistics of atomic frequency standards*, in Proceedings of the *IEEE*, vol. 54, no. 2, pp. 221-230, Feb. 1966, doi: 10.1109/PROC.1966.4634.

[31] W. J. Riley, *Handbook of frequency stability analysis*, *NIST* Special publication 1065, July 2008.

[32] G. Santarelli, C. Audoin, A. Makdissi, P. Laurent, G. J. Dick, et A. Clairon, *Frequency stability degradation of an oscillator slaved to a periodically interrogated atomic resonator*, *IEEE Transactions on Ultrasonics, Ferroelectrics, and Frequency Control* **45** n 4 (juill. 1998) p. 887-894, doi: 10.1109/58.710548.